Performance Intensification of CO2 Methanation by Co-Feeding Oxygen Over Various Ru-Based Catalysts

Journal of Chemical Engineering of Japan

ISSN: (Print) (Online) Journal homepage: https://www.tandfonline.com/loi/tjce20

Performance Intensification of CO_2 Methanation by Co-Feeding Oxygen Over Various Ru-Based Catalysts

Choji Fukuhara, Nozomu Hirata, Ren Ozaki & Ryo Watanabe

To cite this article: Choji Fukuhara, Nozomu Hirata, Ren Ozaki & Ryo Watanabe (2023) Performance Intensification of CO_2 Methanation by Co-Feeding Oxygen Over Various Ru-Based Catalysts, Journal of Chemical Engineering of Japan, 56:1, 2194327, DOI: 10.1080/00219592.2023.2194327

To link to this article: https://doi.org/10.1080/00219592.2023.2194327

Published online: 10 Apr 2023.

JOURNAL OF CHEMICAL ENGINEERING OF JAPAN
2023, VOL. 56, NO. 1, 2194327
https://doi.org/10.1080/00219592.2023.2194327

Taylor & Francis
Taylor & Francis Group

RESEARCH ARTICLE

OPEN ACCESS Check for updates

Performance Intensification of CO_2 Methanation by Co-Feeding Oxygen Over Various Ru-Based Catalysts

Choji Fukuhara[a,b], Nozomu Hirata[b], Ren Ozaki[a], and Ryo Watanabe[a]

[a]Department of Applied Chemistry and Biochemical Engineering, Graduate School of Engineering, Shizuoka University, 3-5-1 Johoku, Naka-ku, Hamamatsu, Shizuoka, 432-8561, Japan; [b]Graduate school of Science and Technology, Shizuoka University, 3-5-1 Johoku, Naka-ku, Hamamatsu, Shizuoka, 432-8561, Japan

ABSTRACT

Auto-methanation (AM), which autonomously progresses at room temperature (approximately 25 °C), is an effective reaction for converting CO_2 to CH_4 and can thus reduce the processing costs. In this study, the AM reaction over various Ru-based catalysts with different support materials positively proceeded by selecting reaction conditions such as the O_2 concentration and gas flow rate. The progression of AM was the best over the Ru/CeO_2 catalyst, followed by the Ru/ZrO_2 and Ru/Al_2O_3 catalysts. The progression of AM over the Ru/SiO_2 catalyst was slow. The rapid progress of AM over the Ru/CeO_2 catalyst was attributed to the presence of oxygen defects on the CeO_2 support that accelerates the hydrogen–oxygen combustion as well as to the differences in the CO_2 and H_2O adsorption characteristics between the CeO_2 support and other supports. Even when the Ru-based catalyst underwent H_2 reduction at low temperature, AM could proceed over each catalyst. The Ru/CeO_2 catalyst was advantageous over other catalysts because AM proceeds only when H_2 gas is supplied at room temperature without external heating. X-ray photoelectron spectroscopy indicated that the Ru species on the Ru/CeO_2 catalyst are in a metallic state owing to H_2 reduction at room temperature, which is associated with AM progression. Moreover, AM proceeded via H_2 reduction at 75 °C over the Ru/ZrO_2 catalyst and at 150 °C over the Ru/Al_2O_3 catalyst. The progression of methanation through such low-temperature reduction can strengthen the CO_2 conversion process.

ARTICLE HISTORY
Received 4 March 2022
Accepted 20 December 2022

KEYWORDS
Auto-methanation; Ruthenium catalyst; CO_2 utilization; Ceria support; Oxygen vacancy

1. Introduction

The development of process technologies related to the reduction and utilization of greenhouse gases is an important research field from the perspective of global environmental conservation. Research on carbon capture and storage (CCS) and carbon capture and utilization (CCU) for the purpose of CO_2 reduction has been actively conducted, and large-scale projects have been promoted in recent years. Jupiter 1000 (https://www.jupiter1000.eu/), STORE & GO (https://www.storeandgo.info/), and ALIGN CCUS (https://www.alignccus.eu/) in Europe are examples of such projects. As CO_2 reduction and utilization techniques, methanol synthesis and dimethyl ether synthesis from CO_2 and H_2 are taken up in the ALIGN CCUS project, and CO_2 methanation is taken up in the Jupiter 1000 and STORE & GO projects.

CO_2 methanation ($CO_2 + 4H_2 \rightarrow CH_4 + 2H_2O$, $\Delta H^0_{298} = -165$ kJ/mol) is a reaction that Paul Sabatier reported in the early 20th century (Sabatier and Senderens 1902). Recently, it has received attention as a reaction that reduces CO_2 emitted from industrial processes and produces a resource such as methane. In this reaction, CO_2 is converted to CH_4 via reduction with eight electrons. For accelerating the reaction, many studies have used a Ni-based, Ru-based, or Co-based catalyst while supplying thermal energy of 250–400 °C to the reaction field. However, the reduction of the supplied thermal energy, that is, the reduction of the reaction temperature, during methanation is challenging. To solve this problem, research on the development of high-performance catalysts is being actively conducted from the viewpoint of catalyst design, which mainly involves selection of the active components and catalyst preparation methods. Concrete studies have been summarized in several review articles based on the development of methanation catalysts (Ghaib et al. 2016; Rönsch et al. 2016; Younas et al. 2016; Frontera et al. 2017; Ashok et al. 2020; Lee et al. 2021). Although there are differences in reaction conditions and catalyst bed conditions, accelerating methanation at approximately 200 °C is one of the development goals for designing low-temperature catalysts.

Additionally, for the treatment of CO_2 emitted from industrial processes by methanation, the development of a catalytic reaction system that enables the handling of a large

CONTACT Choji Fukuhara fukuhara.choji@shizuoka.ac.jp

amount of CO_2 gas and the efficient control of the large amount of exothermic energy associated with the reaction is imperative. These functions are not exhibited by conventional catalyst packed-bed systems, rendering them unsuitable for industrial CO_2 treatment. To address the aforementioned challenges, we have developed a structured catalyst system with excellent heat transfer and a lower pressure loss during the reaction (Fukuhara and Igarashi 2004, 2005; Fukuhara et al. 2005, 2007; Fukuhara and Ohkura 2008; Fukuhara and Kawamorita 2009; Fukuhara et al. 2013, 2015). This is a honeycomb- or spiral-type structured catalyst system onto which an Ni- or Cu-based catalyst component is attached. We reported that this catalytic system allows efficient control of thermal energy and processing of large amounts of CO_2 and is advantageous for deployment in industrial processes (Fukuhara et al. 2017; Ratchahat et al. 2018; Fukuhara et al. 2019). Structured catalysts include the foam-type, plate-type, and sponge-type catalysts; the methanation characteristics of these catalysts were reviewed by Huynh and Yu (2020). From the viewpoint of efficient control of the exothermic energy of methanation, the utilization of a microreactor system is an effective method. Because this reactor system is compact, the exothermic energy and mass transfer of the raw-material gas can be controlled relatively easily. It is expected to facilitate intensification of the methanation process.

For accelerating methanation, heat energy is generally supplied to the reaction field by applying a heating device such as an electric furnace from the outside. The external heating method is also widely used for other catalytic reactions. While, we succeeded in accelerating methanation by co-supplying oxygen gas with a raw-material gas and by using the exothermic energy of hydrogen combustion, maintaining a high methane yield (Fukuhara, Ratchahat, Kamiyama et al. 2019; Fukuhara, Ratchahat, Suzuki et al. 2019; Fukuhara et al. 2020; Hirata et al. 2020). Additionally, we discovered that this heating method autonomously activates methanation at room temperature (approximately 25 °C) and have termed this phenomenon as auto-methanation (AM). The exhaust gas from industrial processes contains not only CO_2 but also large amounts of O_2, N_2, CO, and other gases; thus, an additional process for separating and concentrating CO_2 is generally proposed. The maintenance and operation of this separation/enrichment equipment increase the process cost. If the emitted CO_2 gas can be treated by methanation while O_2 and CO are mixed, the separation and concentration processes become unnecessary, simplifying the process equipment and reducing the construction cost. Furthermore, AM leads to process intensification of CO_2 treatment systems, because autonomous activation and operation of methanation in the room-temperature region significantly reduce the running costs. To understand the possible reasons why CH_4 produced via methanation does not burn in the co-supplied O_2 gas, the order of the minimum ignition energy for the hydrogen–oxygen mixed gas and the methane-oxygen mixed gas was considered (Lewis and Elbe 1961). It was found that because the combustion rate of the hydrogen–oxygen mixed gas is rapid, the combustion of the produced methane does not proceed. We experimentally confirmed the flame retardancy of methane in the presence of O_2 in a previous study (Hirata et al. 2020). We have confirmed the occurrence of such an AM phenomenon using Ni-based catalyst and Ru-based catalyst. When the reaction temperature was changed from the higher side to the lower side, AM occurred even at approximately 25 °C (without external heating) over Ni- and Ru-based catalysts with CeO_2, ZrO_2, Al_2O_3, Y_2O_3, SiO_2, and MgO as supports (Fukuhara et al. 2020). Moreover, when the reaction field was maintained at approximately 25 °C from the beginning, AM was confirmed to occur over the Ru/CeO_2 catalyst (Hirata et al. 2020). However, the applicability of other catalysts for AM has not yet been verified.

Therefore, in this study, we investigated the activation characteristics of methanation on the low-temperature range (25–100 °C) by using several Ru-based catalysts with different support materials. Additionally, the relationship between the physicochemical properties of the catalyst and the occurrence of AM was investigated, with a focus on hydrogen combustion. The results indicated that the Ru/CeO_2 catalyst showed the highest activity toward AM, followed by the Ru/ZrO_2 and Ru/Al_2O_3 catalysts, whereas Ru/SiO_2 catalyst showed the lowest activity. One of the reasons why Ru/CeO_2 catalyst is active toward AM is the deficiency of lattice oxygen in the CeO_2 support. Additionally, it was considered that the Ru/CeO_2 catalyst was easily reduced in the room-temperature region (without external heating) to form metallic Ru, which was also responsible for the easy starting of AM.

2. Experimental

2.1 Preparation of ruthenium-based catalyst

The catalysts used in this study were Ru/CeO_2, Ru/ZrO_2, Ru/Al_2O_3, and Ru/SiO_2, which were prepared via the evaporation-to-dryness method. Ruthenium nitrate ($Ru(NO_3)_3$, Tanaka Kikinzoku Kogyo K. K., Ru: 50 g/L) was used as a Ru source. The loading amount of the Ru component was 10 wt% on an oxide support material. The oxide materials were CeO_2 (labeled JRC-CEO-2), ZrO_2 (labeled JRC-ZRO-3), Al_2O_3 (labeled JRC-ALO-8), and SiO_2 (labeled JRC-SIO-4), which were provided by the Catalysis Society of Japan. The evaporation-to-dryness method involved the sequential combination of the stirring reagent in distilled water, the evaporation of the solvent at approximately 80 °C, and the calcination of the power product. The preparation method was described in our previous report (Fukuhara et al. 2020; Hirata et al. 2020).

2.2 Performance test of methanation

The CO_2 methanation performance of the prepared Ru-loaded catalysts was investigated using a conventional flow-type reactor under the atmospheric pressure. The reactor comprised a quartz tube with an inner diameter of 8 mm. The amount of the Ru-loaded catalyst packed into the

reactor ranged from 300 to 750 mg. A three-independent-zone electric furnace (Asahi Rika Co., ARF) was used for supplying heat energy to the reactive zone. The Ru-loaded catalyst was reduced in the reactor with a H_2 stream of 100 mL/min for 1 h. The reduction temperature was changed from room temperature to 500 °C. Herein, "room temperature" implies no external heating. After the reduction of the catalyst, the CO_2 methanation performance was investigated by feeding a raw-material gas into the reactor at room temperature or 50–75 °C. The raw-material gas was composed of CO_2, H_2, O_2, and N_2 (balance). The CO_2 concentration was fixed at 10 vol%, the O_2 concentration was varied from 0 to 10 vol%, and the H_2 concentration was varied from 40 to 60 vol%. The total flow rate of the raw-material gas was varied from 200 to 800 mL/min. The gas hourly space velocity (GHSV) was varied from 24,000 to 96,000 h^{-1}. The conditions of each experiment are shown in the figure sections. To confirm the reproducibility, all performance tests were conducted two or more times under every reaction condition. The outlet gas was analyzed through gas chromatography (GC-8AIT, TCD, Shimadzu). The detected gases were CH_4, H_2O, CO_2, and CO under all reaction conditions. The fed oxygen was completely consumed during the reaction. No other products were detected. In all reaction runs, the carbon-based material balance was almost 100%. Therefore, the CO_2 conversion and product selectivity were calculated according to the carbon content, by using the following equations:

$$\mathrm{CO_2\ conversion\ (\%)} = \left(1 - \frac{\text{Molar exhaust rate of } CO_2 \text{ at the outlet}}{\text{Molar feeding rate of } CO_2 \text{ at the inlet}}\right) \times 100 \quad (2)$$

$$\mathrm{CH_4\ selectivity\ (\%)} = \frac{\text{Molar production rate of } CH_4 \text{ at the outlet}}{\text{Molar rate of carbon} - \text{containing material at the outlet}} \times 100 \quad (3)$$

$$\mathrm{CO\ selectivity\ (\%)} = \frac{\text{Molar production rate of CO at the outlet}}{\text{Molar rate of carbon} - \text{containing material at the outlet}} \times 100 \quad (4)$$

2.3 Physicochemical measurement

The electronic states of the elements on the catalyst surface were measured via X-ray photoelectron spectroscopy (XPS; Axis Ultra DLD, Shimadzu, X-ray source: AlKα (1486.6 eV)). The XPS measurements were performed under *in situ* conditions via hydrogen reduction (temperature: 25–500 °C; holding time: 1 h) in the pretreatment part attached to the device. The specific surface area of the catalyst was measured using the Brunauer–Emmett–Teller (BET) method (3-Flex, Micromeritics) with liquid nitrogen. The amount of Ru loaded was measured via X-ray fluorescence analysis (Supermini200, Rigaku, Inc.). The temperature desorption behaviors of CO_2 and H_2O were determined by using a catalyst evaluation device (TPD, BELCAT II + CATCryo, Microtrac BEL) equipped with a mass spectrometer. The reduction tendency of the catalyst and the metal surface area of Ru were also determined using this device, that is, H_2-TPR and CO-pulse. The crystalline states of the Ru/CeO_2 catalyst before and after the reaction were measured through X-ray diffraction (Ultima IV, Rigaku, Inc.) analysis with CuKα radiation ($\lambda = 1.54$ Å).

3. Results and Discussion

3.1 Startup property of methanation under O_2 co-feeding

First, we investigated the startup characteristics on the low-temperature side (from room temperature to 100 °C) of methanation under the co-feeding of O_2 gas using Ru-based catalysts with support materials of CeO_2, ZrO_2, Al_2O_3, and SiO_2.

Figure 1 presents the CO_2 and O_2 conversions over various Ru-loaded catalysts under a raw-material gas feed with a composition of CO_2:H_2:O_2:N_2 = 10:50:5:35, using an online mass-spectrometry system. The reaction temperatures were set to room temperature, 50 °C, and 75 °C. The quartz tube was packed with 300 mg of catalyst (average particle size of 500 $\mu m\varphi$) and 400 mg of quartz sand, yielding a uniformly diluted catalyst layer. Prior to the reaction, the catalyst was reduced at 500 °C. In Figure 1, the horizontal axis indicates the time on stream, with the start of the feeding of the raw material as the zero point. For the Ru/CeO_2 catalyst at room temperature, CO_2 conversion increased sharply at the moment when the reaction gas was fed, reaching approximately 80% in <2 min. The product was mostly methane, and it was confirmed that AM was rapidly activated over this catalyst. Additionally, O_2 conversion reached 100% when the reaction gas was supplied. Because the product (methane) was not burned, it is considered that the hydrogen–oxygen combustion occurred rapidly and that AM proceeded by utilizing the combustion exothermic energy (Lewis and Elbe 1961; Fukuhara et al. 2020; Hirata et al. 2020). In contrast, the Ru/ZrO_2, Ru/Al_2O_3, and Ru/SiO_2 catalysts did not exhibit methanation activity at room temperature, and AM rarely proceeded over these catalysts. There was no consumption of the supplied O_2, and only a small amount of O_2 was consumed because of the oxidation of the catalyst after the supply of the raw-material gas. The methanation activity of the Ru/ZrO_2 and Ru/Al_2O_3 catalysts on the low-temperature side was examined at the setting temperature of 50 °C. Although it was slower than that of the Ru/CeO_2 catalyst, methanation started after ≥2 min over the Ru/ZrO_2 catalyst and after ≥5 min over the Ru/Al_2O_3 catalyst. The O_2 consumption increased rapidly to 100%. The hydrogen–oxygen combustion proceeded with the assistance of the heat energy at 50 °C (not a large amount) from the outside; thus, methanation successfully started over these catalysts. Over the Ru/SiO_2 catalyst, methanation on the

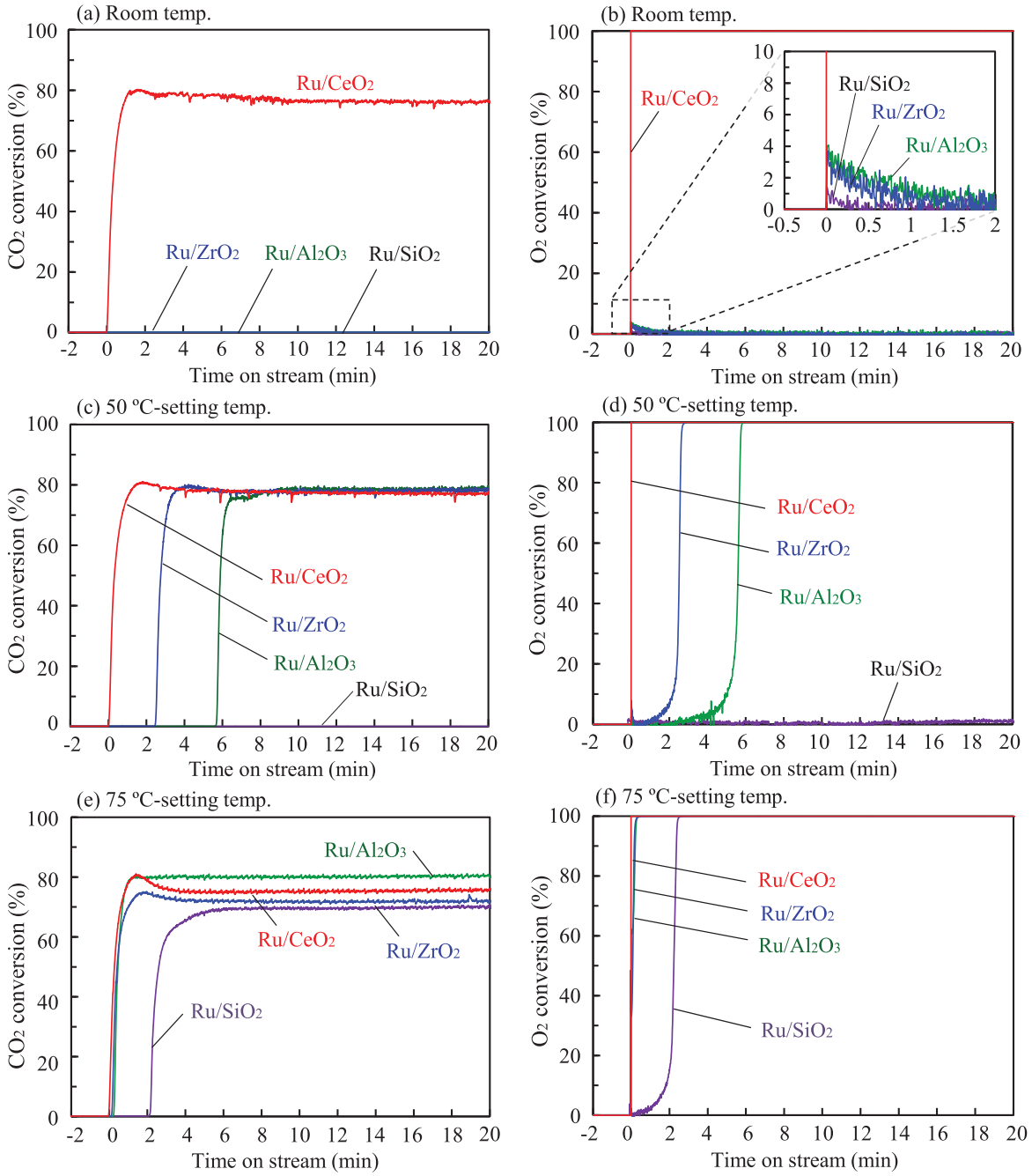

Figure 1. Dynamic starting profiles of methanation (CO_2 and O_2 conversions) at (a), (b) room temperature, (c), (d) 50 °C, (e), (f) 75 °C using various Ru-based catalysts.

low-temperature side finally proceeded at the reaction temperature of 75 °C. Additionally, O_2 conversion exhibited a slower rising behavior than those over other catalysts, and the combustion was slow. However, even over the Ru/SiO_2 catalyst, methanation started at a reaction temperature of 75 °C. This is a new finding that has not previously been reported.

It was inferred that one of the reasons for the difference in the activation characteristics of methanation under the O_2 co-supply was the difference in the physicochemical properties of the different support materials. Table 1 presents the physicochemical properties of each catalyst. The Ru/SiO_2 catalyst had the largest specific surface area, followed by the Ru/Al_2O_3 and Ru/CeO_2 catalysts. The Ru/ZrO_2 catalyst had the smallest specific surface area. The amount of Ru loaded was approximately 10 wt% for the Ru/CeO_2 and Ru/Al_2O_3 catalysts and was slightly smaller for the Ru/ZrO_2 and Ru/SiO_2 catalysts. The amount of metal loaded via the

Table 1. Physicochemical property of various Ru-based catalysts.

	B.E.T. surface area (m^2/g-cat)	Amount of Ru (wt%)	Ru crystallite size[a] (nm)	Ru surface area[b] (m^2/g)
Ru/CeO_2	123	10	30.5	16.0
Ru/ZrO_2	90	9	8.8	55.2
Ru/Al_2O_3	134	11	48.0	10.2
Ru/SiO_2	307	7	162	3.0

[a]Calculated using the Scherrer's equation.
[b]Estimated by CO-pulse method.

impregnation method appeared to be affected by the type of support material. The particle size of the supported Ru species was the smallest for the ZrO_2 support; thus, the metal surface area was large. The Ru particle size was the largest for the SiO_2 support, and the metal surface area was small. The Ru species on the CeO_2 and Al_2O_3 supports were located between the two catalysts. The physical characteristics of the catalysts (such as B.E.T. surface area, Ru crystallite size and Ru surface area) were compared with the start state and performance characteristics of AM shown in Figure 1, and no clear correlation among them was observed.

3.2 Factors affecting the startup of methanation

The factors affecting the methanation startup characteristics of each Ru-loaded catalyst under O_2 co-supply were investigated.

Figure 2 shows the monitoring results for the temperature change of each catalyst layer when the CO_2, H_2, and O_2 gases were sequentially supplied to the catalyst layer and the order of the supplied gases was changed. The reaction temperature was 50 °C, and the supply conditions of the raw materials (gas composition and feeding rate) were identical to those of Figure 1. The temperatures at the inlet and outlet of the catalyst layer were measured by a data logger at intervals of 500 ms. In Figure 2, OP1 corresponds to the supply order of $H_2 \rightarrow O_2 \rightarrow CO_2$, OP2 corresponds to $H_2 \rightarrow CO_2 \rightarrow O_2$, and OP3 corresponds to $CO_2 \rightarrow H_2 \rightarrow O_2$. For the Ru/CeO_2 catalyst, the temperature of the catalyst layer increased immediately after the supply of the O_2 gas in all cases. For OP1, the temperature was increased further by supplying the CO_2 gas after the temperature rise due to the supply of O_2. This suggests that the hydrogen–oxygen combustion occurred first, and the subsequent supply of CO_2 proceeds the methanation. For OP2 and OP3, the temperature did not increase before the supply of O_2 but after it, confirming the acceleration of methanation due to the hydrogen–oxygen combustion energy. Similar behavior was observed for the Ru/ZrO_2 and Ru/Al_2O_3 catalysts. However, compared with the case of the Ru/CeO_2 catalyst, there was a time lag of several minutes before the temperature increased after O_2 supply. For OP1, time lags of 30 s for the Ru/ZrO_2 catalyst and 60 s for the Ru/Al_2O_3 catalyst were observed upon the temperature rise after O_2 supply. The hydrogen–oxygen combustion on the catalyst was also affected by the type of support material. For OP2 and OP3 with the Ru/ZrO_2 and Ru/Al_2O_3 catalysts, the time lag was extended to approximately 120 s. In both operations, CO_2 was supplied before O_2. Therefore, it is considered that CO_2 adsorbed on the catalyst surface inhibited the hydrogen–oxygen combustion by forming the formate and formic acid species (Little 1971; Binet et al. 1999; Fukuhara et al. 2017). Because the order of the gas supply affects the reaction characteristics in this way, it is suggested that combustion and methanation proceed on the catalyst surface and that the physicochemical properties of the support materials affect the combustion performance.

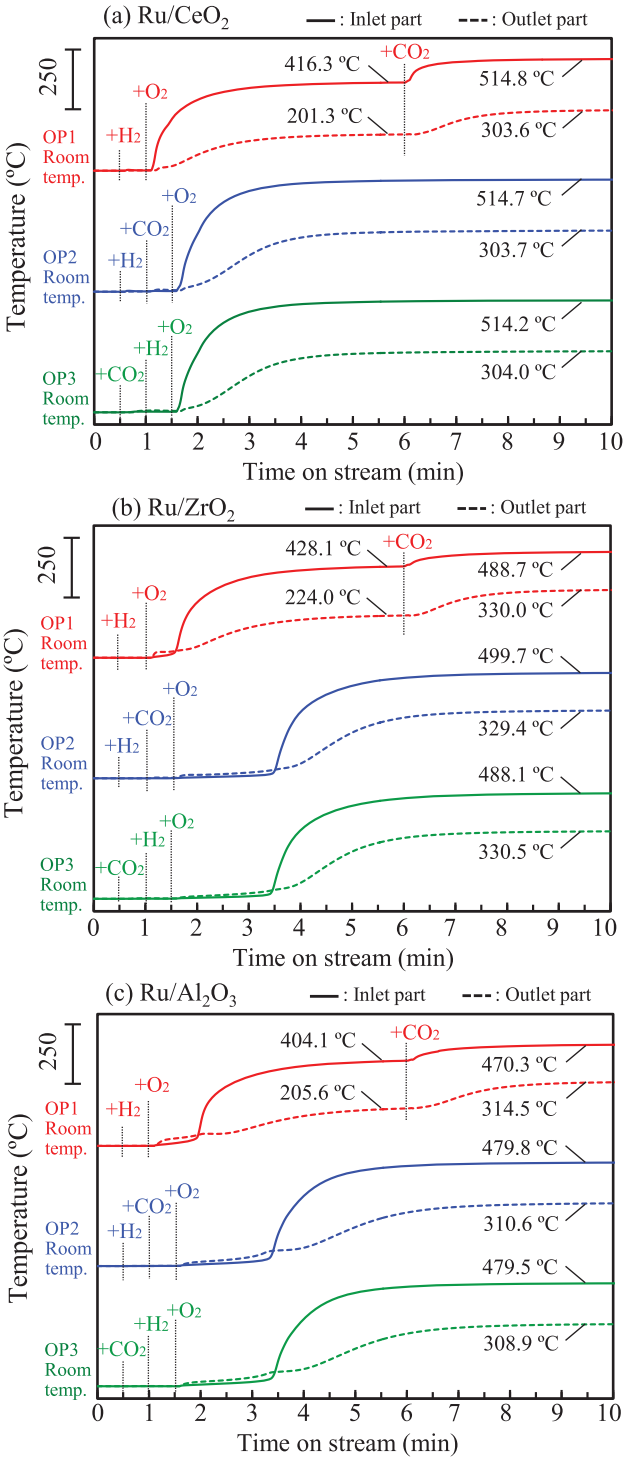

Figure 2. Temperature profile changes of various Ru-based catalyst bed by changing fed order of methanation gas at 50 °C.

Figure 3 shows the XPS profiles of the support element, which were obtained via *in situ* XPS measurements for each Ru catalyst H_2-reduced at 500 °C. In the curve-fitted profile of the CeO_2 support, peaks attributed to Ce^{3+} and Ce^{4+} were observed. It is known that oxygen defects are present on the surface of H_2-reduced CeO_2 (Chen et al. 2009; Wang et al. 2016, 2017; Huang et al. 2018; Li et al. 2019; Zhu et al. 2020). Therefore, the peak attributed to Ce^{3+} indicated that oxygen defects were present on the surface of the prepared Ru/CeO_2 catalyst. In contrast, for the ZrO_2 and Al_2O_3

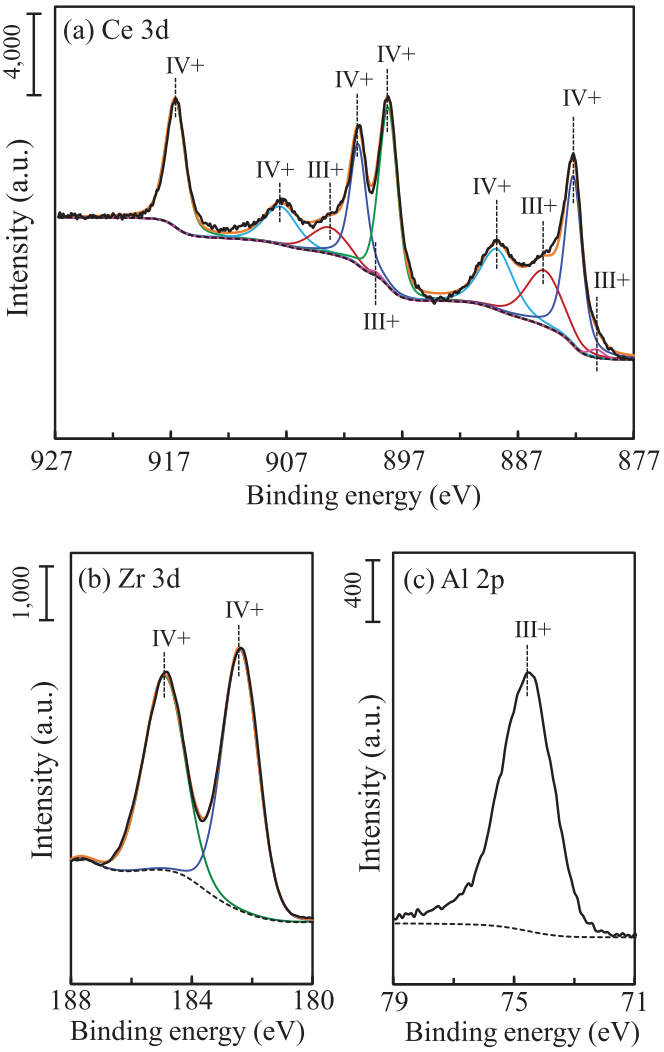

Figure 3. XPS spectra of (a) Ce3d of Ru/CeO_2, (b) Zr 3d of Ru/ZrO_2 and (c) Al 2p of Ru/Al_2O_3 catalysts.

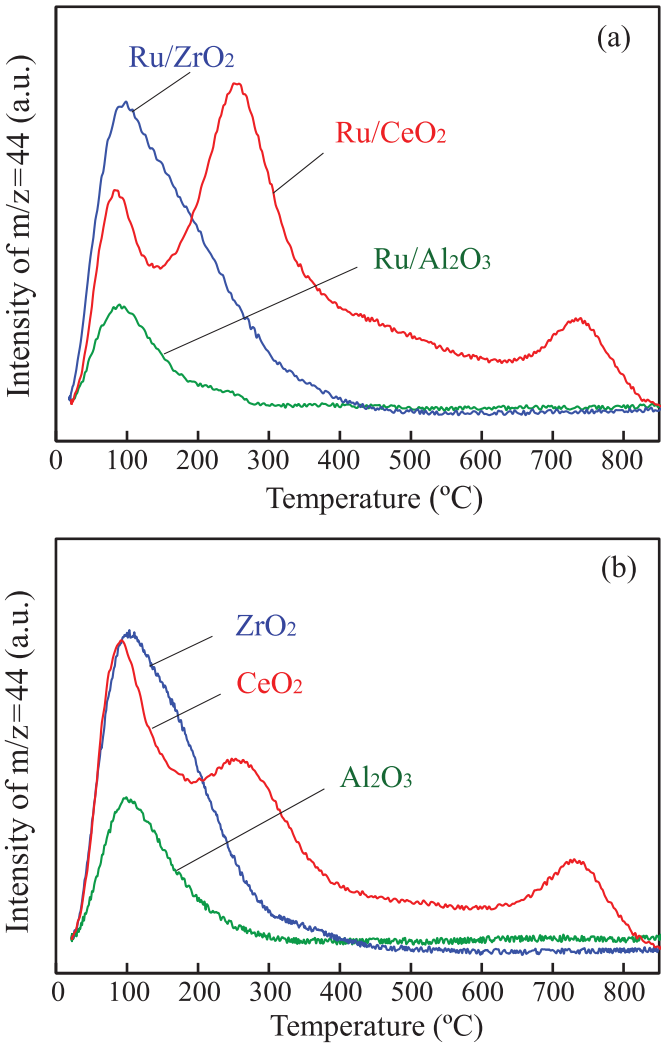

Figure 4. CO_2-TPD profiles of (a) various Ru-based catalysts and (b) support materials.

supports, only Zr^{4+} and Al^{3+} peaks were observed, and there were no other valence elements. The Ru/ZrO_2 and Ru/Al_2O_3 catalysts had no oxygen defects even on the H_2-reduced surface. It has been reported that $Ce^{3+}-V_O^{\cdot\cdot}-Ce^{3+}$ ($V_O^{\cdot\cdot}$: oxygen defect) species are present on the CeO_2 supports having such oxygen defects; O_2 molecules are easily activated at this $V_O^{\cdot\cdot}$ site, and H_2 molecules are smoothly activated on Ce^{3+} (Chen et al. 2009; Huang et al. 2018; Li et al. 2019; Zhu et al. 2020). Thus, the combustion of H_2 rapidly proceeds. In Figure 2, the fact that the combustion proceeded over the Ru/CeO_2 catalyst almost at the same time as the supply of O_2 confirms the relationship between the oxygen-defect site and the combustion property on the catalyst. The rapid starting of H_2 combustion allowed the progression of the AM phenomenon in the room-temperature region shown in Figure 1. However, because there were no oxygen defects on the Ru/ZrO_2 or Ru/Al_2O_3 catalysts, which were the active sites of H_2 combustion, the supplied O_2 was adsorbed on the surface competitively with H_2 and CO_2 molecules. The absence of oxygen defects on both catalysts may be one of the reasons why it took time for the combustion to start after O_2 was supplied for OP1 and why it took more time for OP2 and OP3, where CO_2 was supplied before O_2.

Figure 4 shows the CO_2-TPD profiles for each catalyst. After a reduction treatment at 500 °C, CO_2 was adsorbed on the catalyst surface under a supply of 1 vol% CO_2 (He balance) at 50 °C for 1 h. Subsequently, the signal of CO_2 ($m/z = 44$) was measured using a mass spectrometer while the temperature was increased from 20 to 850 °C at a rate of 10 °C/min under the supply of the He gas. Three peaks were observed for the Ru/CeO_2 catalyst. The peak at approximately 100 °C corresponded to CO_2 adsorbed on weak base sites, and that at 200–350 °C corresponded to CO_2 adsorbed on strong base sites (Luo et al. 1997; Wu et al. 2015; Zhang et al. 2016). The peak at 680–800 °C in the high-temperature range is attributed to CO_2 desorption over the catalyst with lattice oxygen. These peaks were observed in the same temperature range for the CeO_2 support alone, but the peak intensity at 200–350 °C increased when the Ru component was loaded. This temperature range coincides with the temperature range in which methanation activity is accelerated. The increase in the amount of CO_2 adsorbed is considered to be one of the reasons why the Ru/CeO_2 catalyst exhibited high methanation performance. The Ru/CeO_2 catalyst could

adsorb CO_2 not only on the ruthenium element but also on the CeO_2 substrate (Binet et al. 1999; Chen et al. 2009; Panagiotopoulou et al. 2012; Akamaru et al. 2014; Aziz et al. 2015; Wang et al. 2016). Such dual gateways for CO_2 adsorption would bring about increment of adsorbing amount and acceleration of methanation process. The Ru/ZrO_2 catalyst and the ZrO_2 support differed from the Ru/CeO_2 catalyst in that only a large broad peak was observed from the low-temperature side to 300 °C. The Ru/Al_2O_3 catalyst and the Al_2O_3 support exhibited similar profiles. These large peaks corresponded to CO_2 adsorbed on weak or strong base sites on each catalyst (Luo et al. 1997; Bachiller-Baeza et al. 1998; Song et al. 2017; Quindimil et al. 2020). Such a difference in the adsorption state of CO_2 is related to the difference in the startup property of methanation in the presence of oxygen, as shown in Figures 1 and 2.

Figure 5 shows the profiles of H_2O-TPD for each catalyst. After the reduction treatment at 500 °C, H_2O was adsorbed on the catalyst by supplying 5 vol% H_2O (He balance) for 1 h at 50 °C. Then, the H_2O signal was measured using a TCD while the temperature was increased from 20 to 850 °C at a rate of 10 °C/min under He gas supply. The H_2O desorption profiles of the Ru-supported catalysts were almost identical to that of the support alone. The largest amounts of H_2O were desorbed for Ru/Al_2O_3 and Al_2O_3, followed by Ru/ZrO_2 and ZrO_2 and then Ru/CeO_2 and CeO_2. The fact that the Ru/CeO_2 catalyst exhibited the smallest amount of H_2O desorption is attributed to the rapid AM activation on this catalyst. In methanation, in the presence of oxygen, H_2 combustion first occurs over the catalyst, generating H_2O. Because H_2O is a product of methanation, it is preferable that the amount of H_2O is small on the catalyst surface from the viewpoint of the thermodynamic theory. The amount of H_2O generated over the Ru/CeO_2 catalyst was small, and the H_2O was easily desorbed. This feature did not prevent the rapid AM activation over the Ru/CeO_2 catalyst. Conversely, the presence of a relatively large amount of H_2O over the Ru/ZrO_2 and Ru/Al_2O_3 catalysts is considered to be one of the factors that make it difficult for the methanation to proceed.

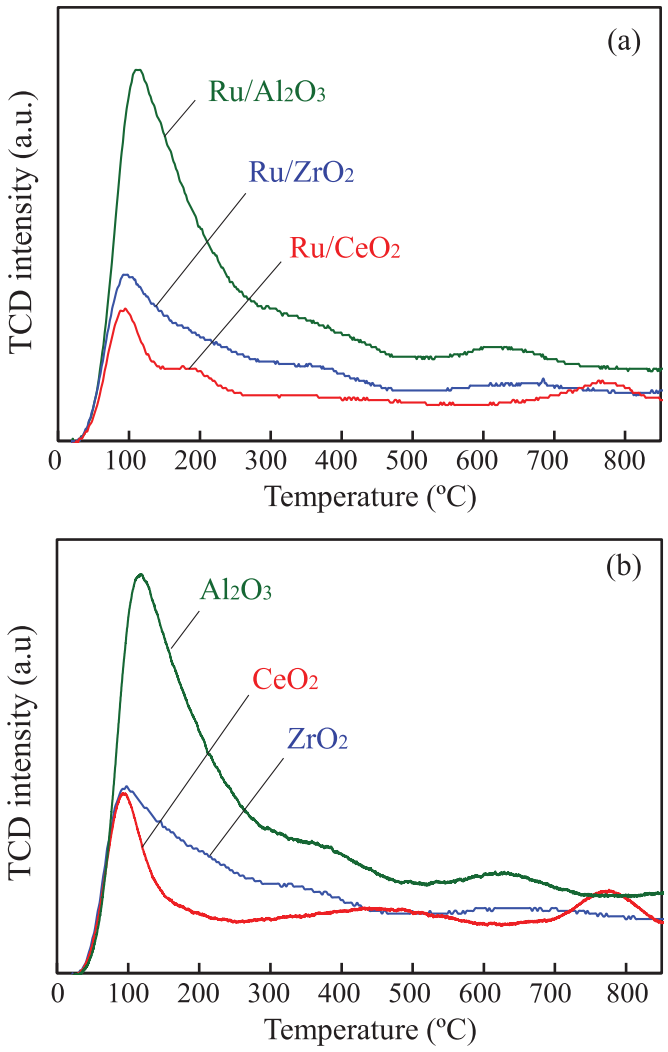

Figure 5. H_2O-TPD profiles of (a) various Ru-based catalysts and (b) support materials.

3.3 Effects of feeding flow rate and O_2 concentration on AM

We previously reported that the AM phenomenon over the Ru/CeO_2 catalyst is affected by the O_2 concentration and the velocity of the gas supplied (Hirata et al. 2020). The same tendency was expected for the Ru/ZrO_2 and Ru/Al_2O_3 catalysts.

Figure 6 shows the effects of changes in the O_2 concentration and gas feeding rate on the AM properties for the Ru/CeO_2, Ru/ZrO_2, and Ru/Al_2O_3 catalysts. All results were obtained at room temperature without external heating. Considering that the AM phenomenon is related to the heat-generation state of the catalyst layer, to standardize the residence time of the supplied gas and to avoid the heat capacity of quartz sand (the diluent), each catalyst layer was set to have a width of 8 mm and a length of 10 mm with only each catalyst component. The packing amounts were 750, 600, and 325 mg for Ru/CeO_2, Ru/ZrO_2, and Ru/Al_2O_3, respectively. The composition of the raw-material gas was CO_2:H_2:O_2:N_2 = 10:42–60:1–10:47–20 (N_2 balance). The flow rate of the gas was varied from 200 to 800 mL/min; thus, the GHSV for this condition varied from 24,000 to 96,000 h^{-1}. In the case of 1 vol% O_2 and the Ru/CeO_2 catalyst, the methanation did not start at any flow rate, but the inlet temperature increased to 50–100 °C. Then, methanation started at a supply rate of 300 mL/min at 2 vol% O_2, and AM occurred at a higher O_2 concentration and gas rate. CO_2 conversion and methane selectivity tended to decrease with the increasing O_2 concentration and gas rate, owing to the equilibrium restriction on the high-temperature side of methanation. The temperature of the reaction field increased as the O_2 concentration and gas rate increased, and a temperature range of ≥600 °C was confirmed. However, an excessive temperature rise causes the detonation phenomenon in the reaction field. Therefore, in CO_2 gas treatment by AM, it is important to select the O_2 concentration and gas supply rate that satisfy the treatment target. Over the

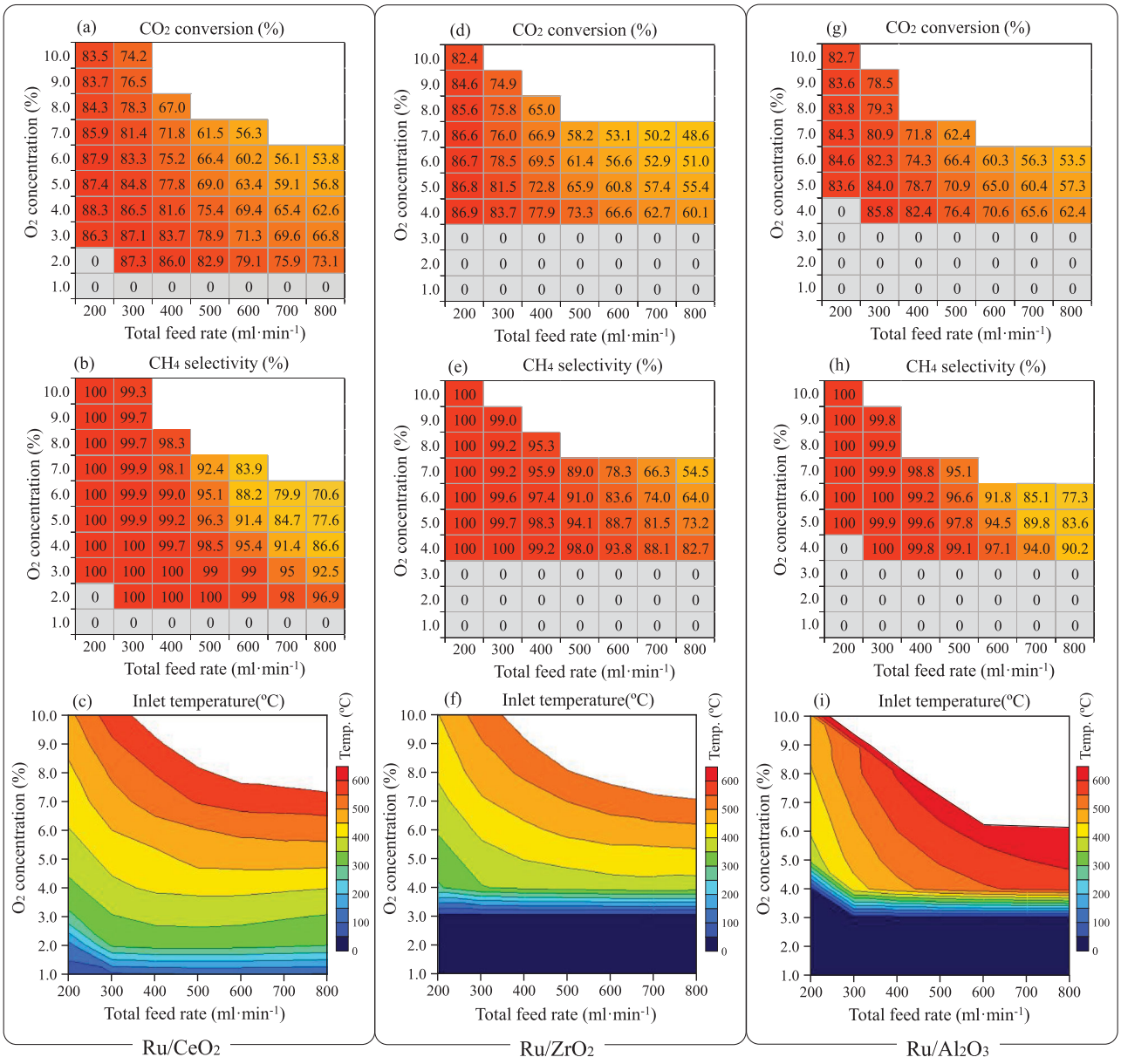

Figure 6. Relationship between auto-methanation property and reaction condition (O_2 concentration and feeding flow rate). (a), (d), (e): CO_2 conversion, (b), (e), (h): CH_4 selectivity and (c), (f), (i): contour profile of inlet temperature (radial center).

Ru/ZrO_2 catalyst, at a concentration of $\leq$3 vol% O_2, methanation did not start at any gas supply rate, and the inlet temperature did not increase. The small amount of catalyst may have been responsible for this result. However, at $\geq$4 vol% O_2, methanation was activated at any gas supply rate, and AM in the room-temperature region progressed even over the Ru/ZrO_2 catalyst. This tendency was also observed for the Ru/Al_2O_3 catalyst, and the AM reaction started at $\geq$4 vol% O_2 and $\geq$300 mL/min. Thus, the Ru/CeO_2 catalyst was the easiest to activate, but the fact that AM in the room-temperature region also occurred over the Ru/ZrO_2 and Ru/Al_2O_3 catalysts implies a wide range for catalyst selection. Regarding the temperature profile of the catalyst layer, it appears that the Ru/ZrO_2 catalyst had many low regions and the Ru/Al_2O_3 catalyst had many high regions compared with the Ru/CeO_2 catalyst. Physicochemical properties such as heat capacity of the support materials may have contributed to this difference.

3.4 Effects of H_2-reduction temperature on AM

It is generally known that the reduction temperature of the catalyst affects its activity. Thus, the effect of the reduction temperature of the Ru-based catalyst on AM was investigated by changing the support materials.

Figure 7 shows the effect of the H_2 reduction temperature on the starting state of AM with the Ru/CeO_2, Ru/ZrO_2, and Ru/Al_2O_3 catalysts. In all experiments, no external heating was performed during methanation. The catalyst layer

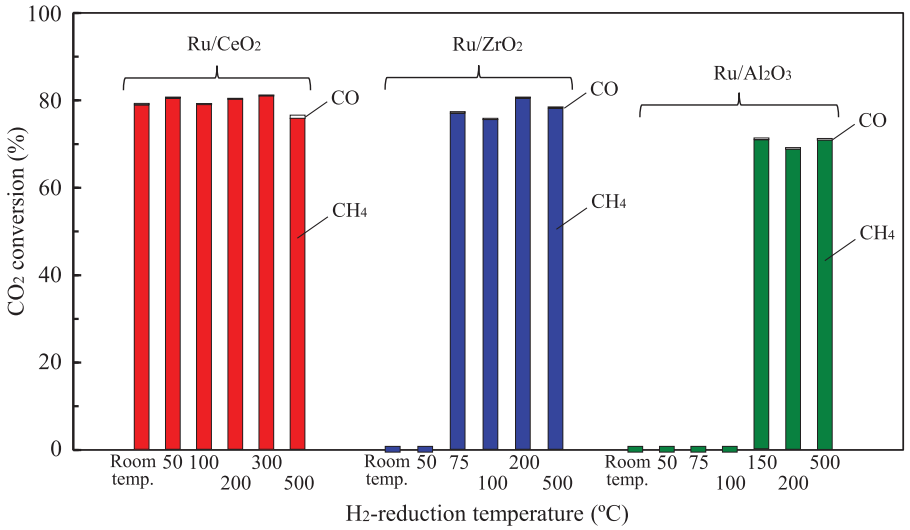

Figure 7. Effect of H_2-reduction temperature on auto-methanation progression over each Ru-based catalyst.

was not diluted with quartz sand and had a diameter of 8 mm and a length of 10 mm, as in the case of Figure 6. The composition of the raw-material gas was CO_2:H_2:O_2:N_2 = 10:50:5:35, and the feeding rate was 400 mL/min. In the reduction operation, N_2 was flowed at the time of the temperature rise, and the H_2 gas (flow rate 100 mL/min) was supplied for 1 h after each reduction temperature was reached (from 50 to 500 °C). Then, the temperature was reduced to room temperature, and the raw-material gas was supplied after the state of the catalyst layer was stabilized. In the case of reduction at room temperature, only the H_2 gas was supplied to the catalyst layer, without external heating. The Ru/CeO_2 catalyst exhibited a conversion of approximately 80% and a methane selectivity of approximately ≥99.5% (a small amount of CO byproduct) at all reduction temperatures. Remarkably, it is a new discovery that the Ru/CeO_2 catalyst exhibited high AM performance with the reduction treatment in which H_2 alone was fed at room temperature, without external heating. The fact that such high AM activity was observed in the reduction treatment that did not require external heating energy confirms the superiority of the Ru/CeO_2 catalyst from the viewpoint of the economic efficiency of process operation. In contrast, the Ru/ZrO_2 and Ru/Al_2O_3 catalysts exhibited the AM activity with the reduction treatment in the presence of external heating energy. However, the Ru/ZrO_2 catalyst exhibited AM activity at a reduction temperature of ≥75 °C, whereas the Ru/Al_2O_3 catalyst led to AM activity at a reduction temperature of ≥150 °C, while maintaining a high performance of 70% to 80%. The advantage of the AM reaction conducted under oxygen supply is that the catalytic activity occurred even for the reduction treatment at temperatures of 75 and 150 °C and even over the Ru/ZrO_2 and Ru/Al_2O_3 catalysts.

Figure 8 shows the results of H_2-TPR measurement for each Ru-based catalyst. The catalysts were oxidized at 300 °C for 1 h under O_2 gas flow and then cooled to −50 °C. After the catalyst bed became stable, the temperature was increased to 750 °C at 10 °C/min while feeding 4 vol% H_2

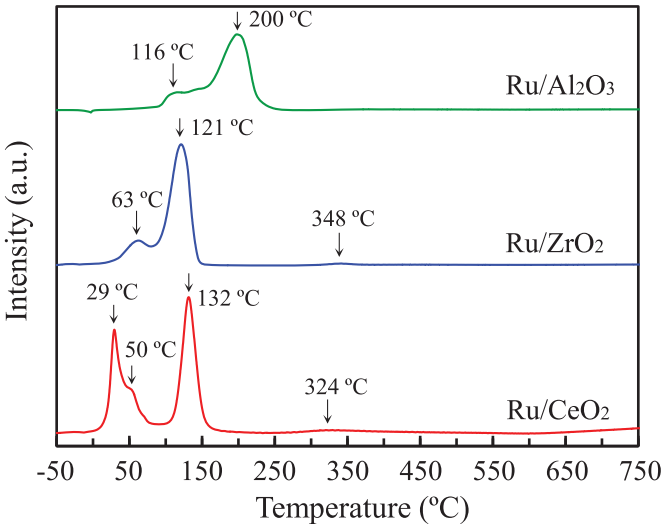

Figure 8. H_2-TPR profiles of various Ru-based catalysts.

(N_2 balance) at 50 mL/min. For the Ru/CeO_2 catalyst, a peak in the range of 20–70 °C and another in the range of 110–150 °C were observed. These peak profiles were clear. A weak broad peak over the range of 300–380 °C was also observed. The peak on the low-temperature side of 20–70 °C corresponded to the RuO_x species, which were well-dispersed on the support, and the peak at 110–150 °C corresponded to the RuO_x species, which aggregated in the bulk (Wang et al. 2009; Guo et al. 2018). The broad peak at 300–380 °C corresponded to the Ru species, which had a strong interaction with the support. For the Ru/ZrO_2 catalyst, the peak profiles could be divided into three temperature ranges. However, the peak in the lowest temperature range was shifted to 45–80 °C, and its intensity was low. Because the peak states of the other two temperature ranges were almost identical, it is suggested that the dispersibility of the RuO_x species corresponding to the peak at 45–80 °C was lower than that of the Ru/CeO_2 catalyst. The peak profile obtained with the Ru/Al_2O_3 catalyst was shifted to the higher-

temperature side compared with those of the other two catalysts. The RuO_x species on this catalyst were not well-dispersed, which was confirmed by scanning electron microscopy in a previous study (Fukuhara et al. 2020). The TPR results indicated that the prepared Ru-based catalyst contained RuO_x species that were easily reduced on the low-temperature side. The reduction-temperature range was of the following order: $Ru/CeO_2 < Ru/ZrO_2 < Ru/Al_2O_3$. This order is consistent with the AM startability trend shown in Figure 7. The Ru species on the Ru/CeO_2 catalyst formed metallic Ru even under H_2 reduction in the room-temperature region without external heating and served as active sites whereat AM progressed. In contrast, the Ru species on the Ru/ZrO_2 catalyst were not reduced by H_2 reduction in the room-temperature region; the metal Ru species were formed at 75 °C, and the AM proceeded. Similarly, the Ru species on the Ru/Al_2O_3 catalyst must be reduced at a higher temperature than those on the Ru/CeO_2 and Ru/ZrO_2 catalysts, and the H_2-reduction treatment at 150 °C promoted AM. It is considered that the difference in the reducing characteristics of the RuO_x species due to the difference in the support materials was related to the AM activity.

In situ XPS measurements of each catalyst were performed to investigate the electronic states of the Ru species on the support. Figure 9 shows profiles of the Ru species of the Ru/CeO_2, Ru/ZrO_2, and Ru/Al_2O_3 catalysts treated at different reduction temperatures. In the catalyst, before reduction (as made), peaks attributed to Ru^{4+} and Ru^{n+} ($0 < n < 4$) were observed for all supports (Elmasides et al. 1999; Chakroune et al. 2005; Yuan et al. 2015; Ma et al. 2017; Hu et al. 2018). The peak profiles were affected by the H_2-reduction treatment, that is, by the reduction temperature. The profiles also depended on the support type. For the Ru/CeO_2 catalyst, a peak of 280 eV belonging to Ru^o species was confirmed by the reduction treatment in the room-temperature region, which corresponded to the peak on the low-temperature side shown in Figure 8 for H_2-TPR. As the reduction temperature increased, the intensity of the peak belonging to the Ru^o species increased, and the intensity of the peak of the Ru^{4+} species decreased. At a reduction temperature of 500 °C, the peak of the Ru^o species was dominant. For the Ru/ZrO_2 catalyst, the peak of the Ru^o species was not observed at reduction temperatures of ≤50 °C but was observed at ≥100 °C. Similarly, for the Ru/Al_2O_3 catalyst, Ru^o species were not detected at reduction temperatures of ≤50 °C but were detected at ≥100 °C. These results are consistent with the AM progression over the Ru/CeO_2 catalyst with a low reduction temperature, as shown in Figure 7. The easy-reduction property of the Ru/CeO_2 catalyst in the room-temperature region may be related to physicochemical properties, such as oxygen defects and CO_2- and H_2O-adsorption properties. This can be investigated in a future study.

4. Conclusions

The AM reaction over various Ru-based catalysts with different support materials positively proceeded by selecting the reaction conditions, such as O_2 concentration and gas flow rate. The Ru/CeO_2 catalyst exhibited the highest catalytic activity, followed by the Ru/ZrO_2 and Ru/Al_2O_3 catalysts. The progression of AM over the Ru/SiO_2 catalyst was slow. As well as to the difference in adsorption characteristics between CO_2 and H_2O, the rapid progress of AM over the Ru/CeO_2 catalyst was attributed to the oxygen defects

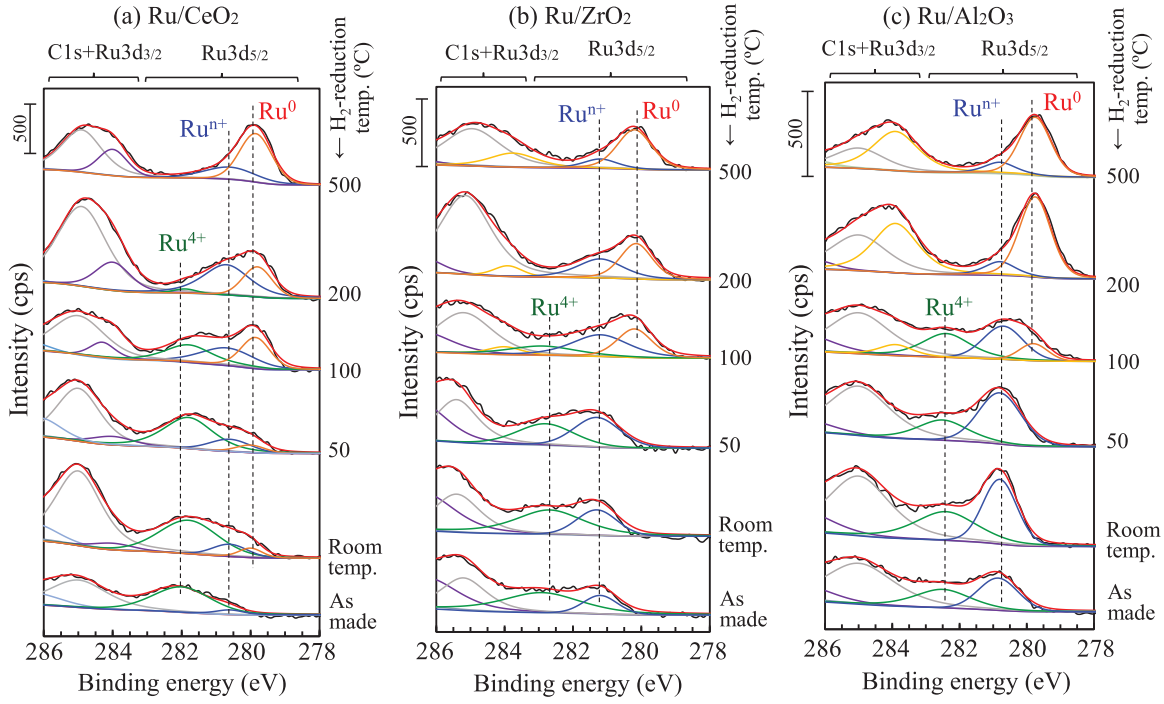

Figure 9. XPS spectra of Ru element for (a) Ru/CeO_2, (b) Ru/ZrO_2 and (c) Ru/Al_2O_3 catalysts with different H_2-reduction temperature.

($Ce^{3+}-V_0^{\cdot\cdot}-Ce^{3+}$) species on the CeO_2 supports that accelerated the hydrogen–oxygen combustion; O_2 molecules are easily activated at this $V_O^{\cdot\cdot}$ site, and H_2 molecules are smoothly activated on Ce^{3+}. AM proceeded over each Ru-based catalyst even when the catalyst was H_2-reduced at a low temperature. The Ru/CeO_2 catalyst was advantageous over the other catalysts because the AM proceeded under the supply of the H_2 gas alone in the room-temperature region without external heating. XPS results indicated that metal Ru species were formed on the Ru/CeO_2 catalyst by H_2 reduction in the room-temperature region and were associated with the progression of AM. The progress of methanation by H_2 reduction at such a low temperature strengthens the CO_2 conversion process.

Disclosure statement

No potential conflict of interest was reported by the author(s).

Funding

This research was supported by JSPS Grant Number 19K22926 and 20H00642.

References

Akamaru S, Shimazaki T, Kubo M, Abe T. 2014. Density functional theory analysis of methanation reaction of CO_2 on Ru nanoparticle supported on TiO_2(101). Appl Catal, A. 470:405–411. doi: 10.1016/j.apcata.2013.11.016

Ashok J, Pati S, Hongmanorom P, Tianxi Z, Junmei C, Kawi S. 2020. A review of recent catalyst advances in CO_2 methanation processes. Catal. Today. 356:471–489. doi: 10.1016/j.cattod.2020.07.023

Aziz MA, Jalil AA, Triwahyono S, Ahmad A. 2015. CO_2 methanation over heterogenious catalysts: recent progress and future prospects. Green Chem. 5:2647–2663.

Bachiller-Baeza B, Rodriguez-Ramos B, Guerrero-Ruiz A. 1998. Interaction of Carbon Dioxide with the Surface of Zirconia Polymorphs. Langmuir. 14:3556–3564. doi: 10.1021/la970856q

Binet C, Daturi M, Lavalley JC. 1999. IR study of polycrystalline ceria properties in oxidized and reduced state. Catal. Today. 50:207–225. doi: 10.1016/S0920-5861(98)00504-5

Chakroune N, Viau G, Ammar S, Poul L, Veautier D, Chehimi MM, Mangeney C, Villain F, Fiévet F. 2005. Acetate- and thiol-capped monodisperse ruthenium nanoparticles: XPS, XAS, and HRTEM studies. Langmuir. 21:6788–6796. doi: 10.1021/la050706c

Chen HT, Chang JG, Chen HL, Ju SP, Comput J. 2009. Identifying the O_2 diffusion and reduction mechanisms on CeO_2 electrolyte in solid oxide fuel cells: A DFT + U study. J Comput Chem. 30:2433–2442. doi: 10.1002/jcc.21247

Elmasides C, Kondarides DI, Grünert W, Verykios XE. 1999. XPS amd FT-IR study of Ru/Al_2O_3 and Ru/TiO_2 catalysts: reduction characteristics and interaction with a methane-oxygen mixture. J Phys Chem B. 103:5227–5239. doi: 10.1021/jp9842291

Frontera P, Macario A, Ferraro M, Antonucci P. 2017. Supported catalysts for CO_2 methanation: a review. Catalysts. 7:59. doi: 10.3390/catal7020059

Fukuhara C, Hayakawa K, Suzuki Y, Kawasaki W, Watanabe R. 2017. A novel nickel-based structured catalyst for CO_2 methanation: A honeycomb-type Ni/CeO_2 catalyst to transform greenhouse gas into useful resources. Appl. Catal. A: Gen. 532:12–18. doi: 10.1016/j.apcata.2016.11.036

Fukuhara C, Hyodo R, Yamamoto K, Masuda K, Watanabe R. 2013. A novel nickel-based catalyst for methane dry reforming: A metal honeycomb-type catalyst prepared by sol-gel method. Appl. Catal A: Gen. 468:18–25. doi: 10.1016/j.apcata.2013.08.024

Fukuhara C, Igarashi A. 2004. Characterization of performance of the wall-type reactor with plate-fin type nickel catalyst prepared by electroless plating, for methanol decomposition. J Chem Eng Japan/JCEJ. 37:415–421. doi: 10.1252/jcej.37.415

Fukuhara C, Igarashi A. 2005. Performance simulation of a wall-type reactor in which exothermic and endothermic reactions proceeded simultaneously, comparing with that of a fixed-bed reactor. " Chem. Eng. Sci. 60:6824–6834. doi: 10.1016/j.ces.2005.06.003

Fukuhara C, Kamata Y, Igarashi A. 2007. Catalytic performance of plate-type Pd/Zn-based catalysts for steam reforming of methanol, prepared by electroless plating. Appl Catal A Gen. 330:108–116. doi: 10.1016/j.apcata.2007.06.037

Fukuhara C, Kamiyama A, Itoh M, Hirata N, Ratchahat S, Sudoh M, Watanabe R. 2020. Auto-methanation for transition-metal catalysts loaded on various oxide supports: a novel route for CO_2 transformation at room-temperature and atmospheric pressure. Chem Eng Sci. 219:115589. doi: 10.1016/j.ces.2020.115589

Fukuhara C, Kawamorita K. 2009. A structured catalyst: noble metal supported on a plate-type zirconia substrate prepared by anodic oxidation for steam reforming of hydrocarbon. Appl Catal A Gen. 370:42–49. doi: 10.1016/j.apcata.2009.09.009

Fukuhara C, Ohkura H. 2008. Physicochemical properties of a plate-type copper-based catalyst, prepared on an aluminum plate by electroless plating, for steam reforming of methanol and CO shift reaction. Appl Catal A Gen. 344:158–164. doi: 10.1016/j.apcata.2008.04.016

Fukuhara C, Ohkura H, Gonohe K, Igarashi A. 2005. Low-temperature water-gas shift reaction of plate-type copper-based catalysts on an aluminum plate prepared by electroless plating. Appl Catal A Gen. 279:195–203. doi: 10.1016/j.apcata.2004.10.036

Fukuhara C, Ratchahat S, Kamiyama A, Sudoh M, Watanabe R. 2019. Auto-methanation performance of structured Ni-type catalyst for CO_2 transformation. Chem Lett. 48:441–444. doi: 10.1246/cl.190025

Fukuhara C, Ratchahat S, Suzuki Y, Sudoh M, Watanabe R. 2019. Auto-methanation of carbon dioxide: a novel route for transforming CO_2 over Ni-based Catalyst. Chem Lett. 48:196–199. doi: 10.1246/cl.180894

Fukuhara C, Yamamoto K, Makiyama Y, Kawasaki W, Watanabe R. 2015. A metal-honeycomb-type structured catalyst for steam reforming of methane: Effect of preparation condition change on reforming performance. Appl Catal A Gen. 492:190–200. doi: 10.1016/j.apcata.2014.11.040

Ghaib K, Nitz K, Ben-Fares FZ. 2016. Chemical methanation of CO_2: a review. ChemBioEng Rev. 3:266–275. doi: 10.1002/cben.201600022

Guo Y, Mei S, Yuan K, Wang DJ, Liu HC, Yan CH, Zhang YW. 2018. Low temperature CO_2 methanation over CeO_2-supported Ru single atoms, nanoclusters, and nanoparticles competitively tuned by strong metal-support interactions and H-spillover effect. ACS Catal. 8:6203–6215. doi: 10.1021/acscatal.7b04469

Hirata N, Watanabe R, Fukuhara C. 2020. Performance characteristics of auto-methanation using Ru/CeO_2 catalyst, autonomously proceeding at room temperature. Fuel. 282:118619. doi: 10.1016/j.fuel.2020.118619

Hu Z, Wang Z, Guo Y, Wang L, Guo Y, Zhang J, Zhan W. 2018. Total oxidation of propane over a Ru/CeO_2 catalyst at low temperature. Environ Sci Technol. 52:9531–9541. doi: 10.1021/acs.est.8b03448

Huang ZQ, Liu LP, Qi S, Zhang S, Qu Y, Chang CR. 2018. Understanding all-solid frustrated-lewis-pair site on CeO_2 from theoretical perspectives. ACS Catal. 8:546–554. doi: 10.1021/acscatal.7b02732

Huynh HL, Yu Z. 2020. CO_2 methanation on hydrotalcite-derived catalysts and structured reactors: a review. Energy Technol. 8:1901475. doi: 10.1002/ente.201901475

Lee WJ, Li C, Prajitno H, Yoo J, Patel J, Yang Y, Lim S. 2021. Recent trend in thermal catalytic low temperature CO_2 methanation: A critical review. Catal. Today. 368:2–19. doi: 10.1016/j.cattod.2020.02.017

Lewis B, Elbe GV. 1961. Combustion, flames and explosions of gases, New York: Academic Press. p. 333–336.

Li Z, Werner K, Qian K, You R, Płucienik A, Jia A, Wu L, Zhang L, Pan H, Kuhlenbeck H, et al. 2019. Oxidation of reduced ceria by incorporation of hydrogen. Angew Chem. 131:14828–14835. doi: 10.1002/ange.201907117

Little LH. 1971. Infrared spectra of adsorbed species. Kagaku Dojin. p. 71–88.

Luo MF, Zhong YJ, Zhu B, Yuan XX, Zheng XM. 1997. Temperature-programmed desorption study of NO and CO_2 over CeO_2 and ZrO_2. Appl Surf Sci. 115:185–189.

Ma Z, Zhao S, Pei X, Xiong X, Hu B. 2017. New insights into the support morphology-dependent ammonia synthesis activity of Ru/CeO_2 catalysts. Catal Sci Technol. 7:191–199. doi: 10.1039/C6CY02089E

Panagiotopoulou P, Kondarides DI, Verykios XE. 2012. Mechanistic aspects of the selective methanation of CO over Ru/TiO_2 catalyst. Catal Today. 181:138–147. doi: 10.1016/j.cattod.2011.05.030

Quindimil A, De-La-Torre U, Pereda-Ayo B, Davó-Quiñonero A, Bailón-García E, Lozano-Gastelló D, González-Marcos JA, Bueno-López A, González-Velasco JR. 2020. Effect of metal loading on the CO_2 methanation: A comparison between alumina supported Ni and Ru catalysts. Catal Today. 356:419–432. doi: 10.1016/j.cattod.2019.06.027

Ratchahat S, Sudoh M, Suzuki Y, Kawasaki W, Watanabe R, Fukuhara C. 2018. Development of a powerful CO_2 methanation process using a structured Ni/CeO_2 catalyst. J CO2 Util. 24:210–219. doi: 10.1016/j.jcou.2018.01.004

Rönsch S, Schneider J, Matthischke S, Schlüter M, Götz M, Lefebvre J, Prabhakaran P, Bajohr S. 2016. Review on methanation - From fundamentals to current projects. Fuel. 166:276–296. doi: 10.1016/j.fuel.2015.10.111

Sabatier P, Senderens JB. 1902. New methane synthesis. Acad Sci. 134:514.

Song F, Zhong Q, Yu Y, Shi M, Wu Y, Hu J, Song Y. 2017. Obtaining well-dispersed Ni/Al_2O_3 catalyst for CO_2 methanation with a microwave-assisted method. Int J Hydrog Energy. 42:4174–4183. doi: 10.1016/j.ijhydene.2016.10.141

Wang F, He S, Chen H, Wang B, Zheng L, Wei M, Evans DG, Duan X. 2016. Active site dependent reaction mechanism over Ru/CeO_2 catalyst toward CO_2 methanation. J Am Chem Soc. 138:6298–6305. doi: 10.1021/jacs.6b02762

Wang M, Weng W, Zheng H, Yi X, Huang C, Wan H. 2009. Oscillations during partial oxidation of methane to synthesis gas over Ru/Al_2O_3 catalyst. J Nat Gas Chem. 18:300–305. doi: 10.1016/S1003-9953(08)60126-7

Wang Y, Yu C, Meng X, Zhao P, Chou L. 2017. The ethanol mediated-CeO_2-supported low loading ruthenium catalysts for the catalytic wet air oxidation of butyric acid. RSC Adv. 7:39796–39802. doi: 10.1039/C7RA06028A

Wu Z, Mann AKP, Li M, Overbury SH. 2015. Spectroscopic Investigation of Surface-Dependent Acid-Base Property of Ceria Nanoshapes. J Phys Chem C. 119:7340–7350. doi: 10.1021/acs.jpcc.5b00859

Younas M, Kong LL, Bashir MJK, Nadeem H, Shehzad A, Sethupathi S. 2016. Recent advancements, fundamental challenges, and opportunities in catalytic methanation of CO_2. Energy Fuels. 30:8815–8831. doi: 10.1021/acs.energyfuels.6b01723

Yuan Q, Zhang D, Haandel LV, Ye F, Xue T, Hensen EJ, Guan Y. 2015. Selective liquid phase hydrogenation of furfural to furfuryl alcohol by Ru/Zr-MOFs. J. Mol. Catal. A: Chem. 406:58–64. doi: 10.1016/j.molcata.2015.05.015

Zhang S, Chang C-R, Huang Z-Q, Li J, Wu Z, Ma Y, Zhang Z, Wang Y, Qu Y. 2016. Solid frustrated-Lewis-pair catalysts constructed by regulations on surface defect of porous nanorods of CeO_2. J Am Chem Soc. 138:2629–2637. doi: 10.1021/jacs.5b11413

Zhu H, Hou Y, Ren H, Liu D, Li X, Zhao L, Chi Y, Guo W. 2020. Theoretical investigation on H_2 oxidation mechanisms over pristine and Sm-doped CeO_2(111) surfaces. Appl Surf Sci. 511:145388. doi: 10.1016/j.apsusc.2020.145388